Superelastic Supercapacitors with High Performances during Stretching

*Zhitao Zhang, Jue Deng, Xueyi Li, Zhibin Yang, Sisi He, Xuli Chen, Guozhen Guan, Jing Ren, and Huisheng Peng**

Wearable electronics and microelectronics have attracted increasing attention to make our life more convenient and less energy-consuming with higher quality in recent decades.[1–4] To satisfy their vigorous advancements in the future, it is critical, while remains challenging, to find matchable energy devices to power them.[5,6] As a result, more and more interests are attracted to develop photovoltaic devices, lithium ion batteries, and supercapacitors in a fiber format aiming at light weight and weaveability in the next-generation electronic products.[7–12] They are proposed to be integrated into clothes or attached directly onto the skin, possibly leading to a technical revolution in electronics. However, these fiber-shaped energy devices have to experience a dramatically stretching process in practical wearable applications. Therefore, it is necessary but unavailable yet to evaluate their properties when they are dynamically stretched. On the other hand, a lot of efforts have been made to fabricate stretchable solar cells, lithium ion batteries, and supercapacitors based on elastic film-based electrodes to meet the flexible and elastic nature in human body.[13–18] Although it is rare to understand how their properties are varied during a dynamically stretching process either, this stretchable strategy provides a useful clue to study the wearable fiber-shaped energy devices.[19] To this end, they are further required to exhibit a combined high stretchability and energy conversion/storage efficiency, e.g., high and stable specific capacitances for fiber-shaped supercapacitors under and after stretching at large strains. However, it remains unavailable yet, which has also been recognized as a bottleneck in the development of the wearable electronics.[17]

Here we have developed a new superelastic fiber-shaped supercapacitor (SFS) that may pave the way for the advancement of applicable miniature energy storage devices. The SFS has been produced by using two aligned carbon nanotube (CNT)/polyaniline (PANI) composite sheets as electrodes and can be stretched by over 400%. As a demonstration, a high specific capacitance of approximately 79.4 F g^{-1} is well maintained after stretching at a strain of 300% for 5000 cycles or 100.8 F g^{-1} after bending for 5000 cycles at a current density of 1 A g^{-1}. The specific capacitance of the SFS can be maintained by 95.8% at a stretching speed as high as 30 mm s^{-1}.

The fabrication of the SFS is schematically shown in Figure S1 (Supporting Information) and **Figure 1**. An elastic polymer fiber electrode is first prepared by winding aligned CNT sheets onto a superelastic fiber in a prestretched state (the prestrain method proves efficient to fabricate superelastic devices[18]), followed by a release to the relaxed state. Here the aligned CNT sheets have been produced from spinnable CNT arrays that are synthesized by chemical vapor deposition.[20–22] A layer of PANI is then deposited onto the CNT sheet after electropolymerization of the monomer, i.e., aniline.[5,23,24] The modified fiber that serves as the inner electrode is then coated with a thin layer of poly (vinyl alcohol) (PVA) gel electrolyte. Another aligned CNT/PANI sheet that is generally prepared by electrodepositing PANI onto a CNT sheet is further wound as the outer electrode. The two composite sheet electrodes share both thickness and weight. The second layer of PVA electrolyte is finally coated to obtain the desired SFS. Repeated stretching–releasing and vacuum treatments are used to improve the infiltration of the electrolyte into the aligned CNT/PANI sheet during the fabrication. Here the aligned CNT sheet serves as both current collector and active material to contribute to the capacitance.

Figure 2a shows a typical scanning electron microscopy (SEM) image of the inner CNT layer that serves as the inner electrode in the SFS. Obviously, the aligned CNT sheet is stably attached onto the fiber substrate, mainly by van der Waals force between the aligned CNTs and elastic fiber substrate.[25] The helical angle of the aligned CNT sheet along the axial direction of the fiber was maintained during the winding process when the precession velocity of the aligned CNT sheet equaled the moving velocity of the translation stage.[10] A layer of aligned CNT sheet displayed an average thickness of approximately 18 nm, and the thickness of the aligned CNT layer on the elastic polymer fiber can be increased and accurately tuned by varying the helical angle and width of the wound aligned CNT sheet (Figure S2, Supporting Information). Figure 2b–d verifies that the CNTs remain highly aligned in the CNT/PANI composite layer. The following coat of the PVA gel electrolyte layer produced a smooth outer surface (Figure 2e). Figure 2f–h shows cross-sectional images of an SFS, and the active layers are uniform in thickness on the surface of the elastic polymer fiber.

To produce a high-performance supercapacitor, it is the key to preparing high-quality electrode materials. A pure elastic polymer fiber that can be stretched by approximately

Z. Zhang, J. Deng, X. Li, Dr. Z. Yang, S. He, X. Chen, G. Guan, J. Ren, Prof. H. Peng
State Key Laboratory of Molecular Engineering of Polymers
Department of Macromolecular Science and Laboratory of Advanced Materials
Fudan University
Shanghai 200438, China
E-mail: penghs@fudan.edu.cn

DOI: 10.1002/adma.201404573

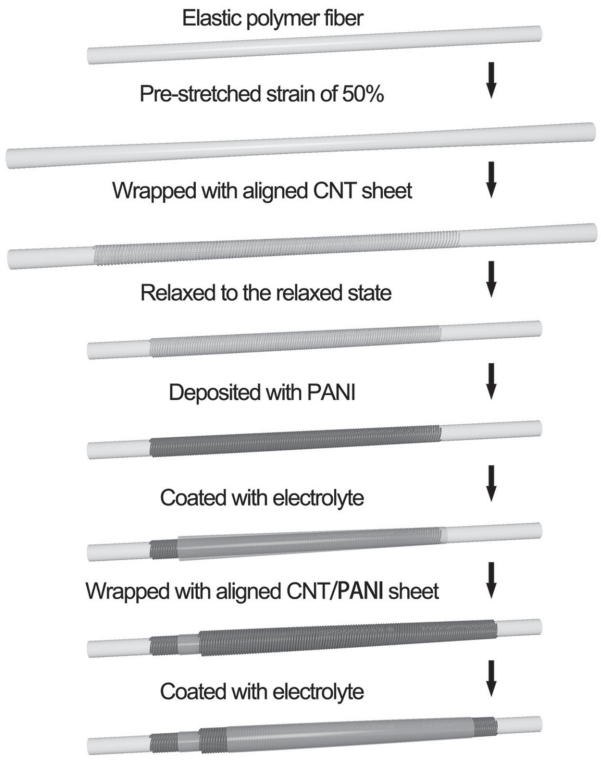

Figure 1. Schematic illustration of the fabrication of an SFS.

900% (Figure S3, Supporting Information) had been carefully made to produce elastic fiber electrodes. The measured diameters are similar to the calculated values, indicating a uniform deformation during stretching (Figure S4, Supporting Information). The detailed diameter calculation on the elastic polymer fiber during stretching is described in the Supporting Information. The maximal strains of elastic fiber electrodes were decreased with increasing helical angles (**Figure 3**a), which may be explained by the soft nature of polymer fibers. After being wound with the aligned CNT sheet, the elastic fiber became smaller in diameter after release compared with the polymer fiber without the CNT sheet on the surface (Figure S5, Supporting Information). In other words, some deformations were fixed to be irreversible by the wrapped CNTs. As expected, the irreversible deformations would be increased at higher helical angles. Since the volume of polymer fiber remained unchanged, the resulting CNT/polymer fiber became longer with increasing helical angles under the same other conditions such as the same length of used polymer fibers. Therefore, the elongation of the CNT/polymer fiber electrode was increased with the increasing helical angle (Figures S6 and S7, Supporting Information).

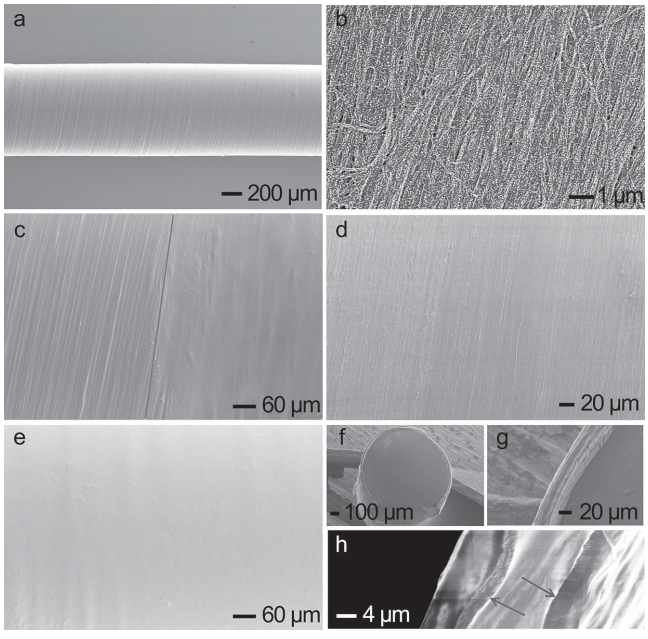

Figure 2. SEM images of the SFS. a) The inner aligned CNT sheet. b) Aligned CNT/PANI sheet. c) After coat with the PVA gel electrolyte. d) After wrapping with aligned CNT/PANI sheet. e) High magnification of an SFS after coat with the PVA gel electrolyte. f–h) Cross-sectional images of an SFS at increasing magnifications. The arrows show the aligned CNT sheet.

Electrical properties of elastic fiber electrodes had been first compared by wrapping aligned CNT sheets with increasing wrapping helical angles from 20° to 80° under the same conditions including the diameter of 1160 μm for the elastic polymer fiber, prestretched strain of 100%, and aligned CNT thickness of approximately 460 nm (Figure S5, Supporting Information). For the elastic fiber electrodes, as the CNT sheets at the sheath part exhibited the same thickness, the electrical resistances of such fiber electrodes were compared mainly on the basis of contact resistances among CNTs without considering the resistances of individual CNTs that were almost the same. As the above contact resistances along the axial direction are increased with increasing helical angles, the resistance of the elastic fiber electrode is also increased from 0.56 to 5.8 kΩ cm^{-1} when the wrapping helical angles are increased from 20° to 80°. Figure 3b has further compared the change of fiber resistances during stretching. As expected, due to the increasing resistances with increasing wrapping helical angles, the changes in resistance are decreased at higher wrapping helical angles under the same strain of 450%. To obtain highly stretchable and stable supercapacitors, a wrapping helical angle of 80° is studied below if not specified.

The electrical properties of elastic fiber electrodes also depend on the prestretched strain (Figure S8, Supporting Information). The resistance changes are calculated as 27.9%, 41.5%, and 35.6% for the elastic fiber electrodes at prestretched strains of 50%, 100%, and 200% upon being stretched by 300%, respectively. The lower resistance at a lower prestretched strain is explained by the formed lower helical angle of the aligned CNTs after release of the fiber electrode (Figure S9, Supporting Information). As previously mentioned, a lower helical angle reduced the resistances of CNT sheets at the same thickness. A lower prestretched strain also enhanced the maximal strain of elastic fiber electrodes (Figure S10, Supporting Information). With the increasing prestretched strain, the elastic fiber electrodes became thinner with increased lengths. Therefore, a prestretched strain of 50% had been used in the following study. The outer surface of the elastic fiber electrode has been further traced under being stretched to 500%, and the CNTs remain highly aligned and stably attached on the fiber substrate (Figure S11, Supporting Information).

ADVANCED MATERIALS
www.advmat.de

www.MaterialsViews.com

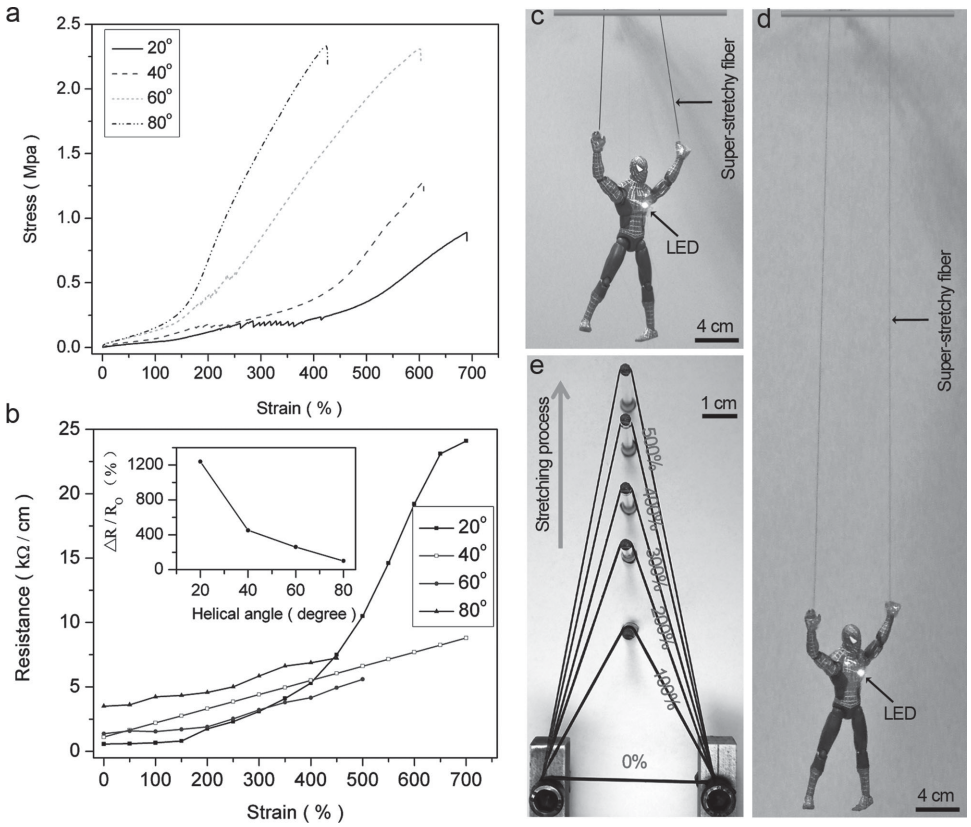

Figure 3. a) Stress–strain curves of elastic fiber electrodes with different wrapping helical angles. b) Dependence of electrical resistance on the strain (inserted, dependence of resistance ratio on wrapping helical angle at the same strain of 450%). R_0 and R correspond to resistances before and after stretching, respectively. c, d) Photographs of the elastic fiber electrode to power a light emission diode before and after stretching by a load, respectively. e) Photograph of an elastic fiber electrode before and after stretching by 100%, 200%, 300%, 400%, and 500%.

Besides the wrapping helical angle and prestretched strain, the resistance of the elastic fiber electrode can also be tuned by varying the thickness of aligned CNT (Figure S12, Supporting Information). The resistances are reduced from 2.32 to 0.18 kΩ cm^{-1} with increasing thicknesses of aligned CNT sheets from 350 nm to 3.5 μm. The resistances are increased below 70% at strains of less than 400% and largely enhanced to 248% at a higher strain of 500% (Figures S13 and S14, Supporting Information). For the investigated thickness range of the CNT sheet, no obvious effect of CNT thickness on the maximal strain was observed. For practical applications, the resistances of fiber electrodes needed to be further decreased. Some effective strategies had been proposed to significantly reduce their resistances by lengthening the CNTs or making a pressurized rolling post-treatment.[26,27] After optimization, the elastic fiber electrodes were highly stable and electrically conductive. They had been connected to lighten up a light-emitting diode (LED) during dramatically stretching (Figure 3c,d). No obvious damages in structure are observed in the fiber electrode under SEM after repeated stretching by 400% (Figure S10, Supporting Information, and Figure 3e).

The SFS is then fabricated from the elastic fiber electrode and PVA gel electrolyte.[28] Figure S15 (Supporting Information) shows galvanostatic charge–discharge curves of the SFS between 0 and 1 V at a current density of 0.1 A g^{-1}. The charge–discharge curves were nearly symmetric, indicating a high reversibility between charge and discharge processes. The specific capacitances are first increased from 18 to 19.6 F g^{-1} with the increasing thickness of CNT layers from 175 to 350 nm and then decreased to 13.2 F g^{-1} with the further increase in thickness. The formation of a platform may be explained by the fact that it is difficult for the PVA gel electrolyte to infiltrate into the inner aligned CNT sheet. The active layer has not been fully used. As a result, the elastic fiber electrode with the CNT thickness of 350 nm shows the best overall performance and is used for the following study. Figure S16 (Supporting Information) has compared galvanostatic charge–discharge profiles of SFSs based on different PANI weight percentages at 1 A g^{-1}, and the maximal specific capacitance appears at 50%. The specific capacitances were gradually enhanced from 31.0 to 105.8 F g^{-1} with the increasing PANI weight percentage from 15% to 50% due to the improved pseudocapacitance from the PANI, and then decreased to 80.3 F g^{-1} due to the decreasing electrical conductivities with the increasing PANI weight percentage to 70%. The maximal specific capacitance corresponded to the length-specific capacitance of 0.90 mF cm^{-1} or area-specific capacitance of 3.08 mF cm^{-2}. The area-specific capacitance can be further enhanced to 50.1 mF cm^{-2} by increasing the electrical conductivity (Figure S17, Supporting Information), and it is much higher than the previous supercapacitors compared in Table S1 (Supporting Information).[29–35] The PANI weight percentage of 50% is discussed below.

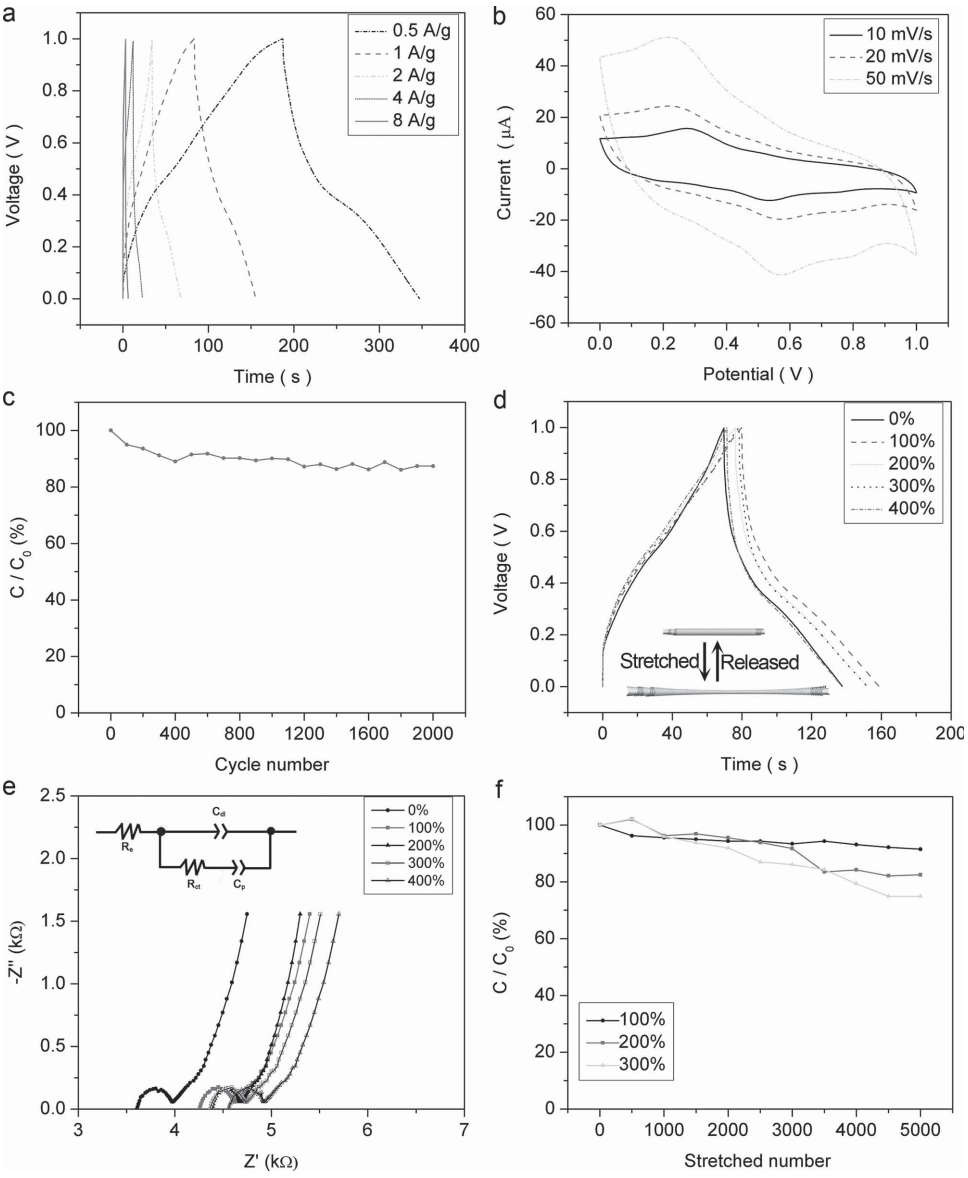

Figure 4. a) Galvanostatic charge–discharge profiles at increasing current densities. b) Cyclic voltammograms with increasing scan rates. c) Dependence of specific capacitance on cycle number at a current density of 1 A g^{-1}. d) Galvanostatic charge–discharge profiles with increasing strains from 0% to 400%. e) Nyquist plots with increasing strains from 0% to 400%. f) Dependence of specific capacitance on stretched number with increasing strains from 100% to 300%. C_0 and C correspond to specific capacitances before and after stretching, respectively. The supercapacitor at a–f) was fabricated with the PANI weight percentage of 50%.

Galvanostatic charge–discharge processes are further carried out at the increasing current densities from 0.5, 1, 2, 4 to 8 A g^{-1} (**Figure 4**a),[36–38] and the capacitances have been maintained by 94.8%, 64.1%, 33.2%, and 12.8%, respectively. The symmetric curves are well maintained, which further verifies the good rate capability. Figure 4b shows cyclic voltammograms with the expected PANI redox peaks for a pseudocapacitance. In addition, the redox peaks are well maintained with the increasing scan rate from 10 to 50 mV s^{-1}, indicating a rapid redox reaction of PANI.[38,39] To investigate the stability of the SFS, a cyclic charge–discharge characterization is carried out at a current density of 1 A g^{-1} (Figure 4c), and the specific capacitances are maintained by 90% after 2000 cycles. Figure 4d shows galvanostatic charge–discharge profiles with increasing strains to 400%, and the specific capacitances remain almost unchanged. Figure S18 (Supporting Information) shows the photograph of the SFS with increasing strains from 0% to 400%. The PANI/CNT composite sheet was also traced by SEM after stretching to 200%, and the structure had not been damaged during the process (Figure S19, Supporting Information). The stable electrochemical performance is also verified by the same shape of Nyquist plots after stretching (Figure 4e). With the increasing strain rate, the equivalent series resistance (calculated from the high-frequency intercept of the semi-circle on the real axis) was slightly increased. Differently, the diameters of semi-circles were similar, indicating that the charge-transfer

Table 1. Comparison of this SFS with previous stretchable supercapacitors in terms of specific capacitance and stretchability.

References	Electrode materials	C		Stretchability [%]
		C_g [F g^{-1}]	C_A [mF cm^{-2}]	
This study	PANI/CNT	111.6 ± 2.3	50.1 ± 1.2	400
17	CNT/OMC	41.4		100
29	CNT		4.99	100
30	Graphene	7.6	0.006	40
42	CNT	59		20
43	PANI/graphene	261		30
44	Polypyrrole	125.1		100
45	CNT	54		30
46	CNT	53		140

Note. CNT: carbon nanotube; OMC: ordered mesoporous carbon; PANI: polyaniline.

resistances between the electrode and electrolyte remained stable.[40,41] Figure 4f shows the dependence of specific capacitance on stretched number with increasing strains from 100% to 300%, and the capacitance has been maintained by 74.9% after stretching for 5000 cycles. The well-maintained structure can also explain the stable electrochemical properties (Figure S20, Supporting Information). Figure S21 (Supporting Information) shows galvanostatic charge–discharge profiles when the SFS was stabilized at the stretched state with different strains, and a high electrochemical performance has been well maintained. Figure S22 (Supporting Information) shows the dependence of specific capacitance on stretched cycle number at the strain of 400%, and the capacitance has been further maintained by 92.8%. As the PVA gel electrolyte could be stretched by 400%, the resulting SFS was stretchable at a strain up to 400%.

The specific capacitance and stretchability of this SFS and previous stretchable supercapacitors are compared in **Table 1**. [17,29,30,42–46] The SFS exhibits a relatively high specific capacitance with the highest strain. As expected, the flexible SFS can be easily woven into textiles also with high electrochemical performances. For instance, the specific capacitances have been maintained by 97% after stretching by 200%, and the deformations are highly reversible (**Figure 5**). In addition, the specific capacitances are maintained by 98.5% even after bending with the curvature of 2 mm (Figure S23, Supporting Information), and they can be further maintained by 95.2% after bending for 5000 cycles (Figure S24, Supporting Information).

Based on the super-stretchy property of the continuous SFS, we had further traced the specific capacitances during a dynamically stretching process with increasing speeds. **Figure 6**a shows that the specific capacitance can be maintained by 95.8% even at a stretching speed as high as 30 mm s^{-1}. Figure 6b shows the dependence of specific capacitance on time under both stretching and releasing at a speed of 10 mm s^{-1}, and the specific capacitance was well maintained, indicating a stable electrochemical performance during the dynamic deformation. The dependence of specific capacitance on stretching and releasing time has also been studied (Figure 6c), and it was varied at below 10% in 500 cycles. Figure 6d displays the applications where a powering textile woven from the SFSs is used to power an LED. The luminance of the light emission diode remained almost unchanged during stretching with increasing speeds up to 30 mm s^{-1}.

A stretchable supercapacitor was proposed by sequentially coating a PVA gel electrolyte and winding an aligned CNT sheet electrode onto a CNT fiber, but it could be stretched at a strain below 75% and repeated for several cycles. A low stretchability of the electrodes prevented the realization of a superelastic supercapacitor. Here the SFS can be stretched by as high as 400%, and the specific capacitance reached 111.6 F g^{-1} at a current density of 0.5 A g^{-1}, compared with 41.4 F g^{-1} of the previous work. In addition, a high specific capacitance of approximately 79.4 F g^{-1} had been well maintained after stretching at a strain of 300% for 5000 cycles or 100.8 F g^{-1} after bending for 5000 cycles at a current density of 1 A g^{-1}. More importantly, the specific capacitance of the SFS can be maintained by 95.8% at a stretching speed as high as 30 mm s^{-1}, which has not been previously explored yet.

In summary, an SFS has been developed with high electrochemical property by winding aligned CNT/PANI sheets onto an elastic polymer fiber. In particular, the SFS, for the first time, is produced for a stable powering performance under dynamically stretching, which paves the way for their practical applications in electronic textiles and various other wearable devices.[32,47,48]

Experimental Section

Preparation of Elastic Fiber Electrode: A precursor solution, Ecoflex 30 (Smooth-On, USA), was injected into a heat-shrinkable tube, followed by curing at 80 °C for 2 h. An elastic polymer fiber was then pulled out of the heat-shrinkable tube. The aligned CNT sheet was wrapped onto

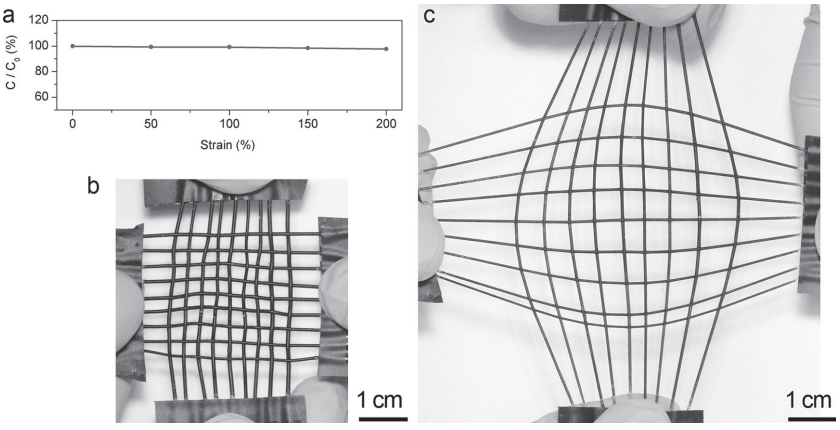

Figure 5. a) Dependence of specific capacitance of the supercapacitor textile on strain. C_0 and C correspond to specific capacitances at 0 and the other strains, respectively. b, c) Photographs of a flexible and stretchable textile before and after stretching by 100%, respectively.

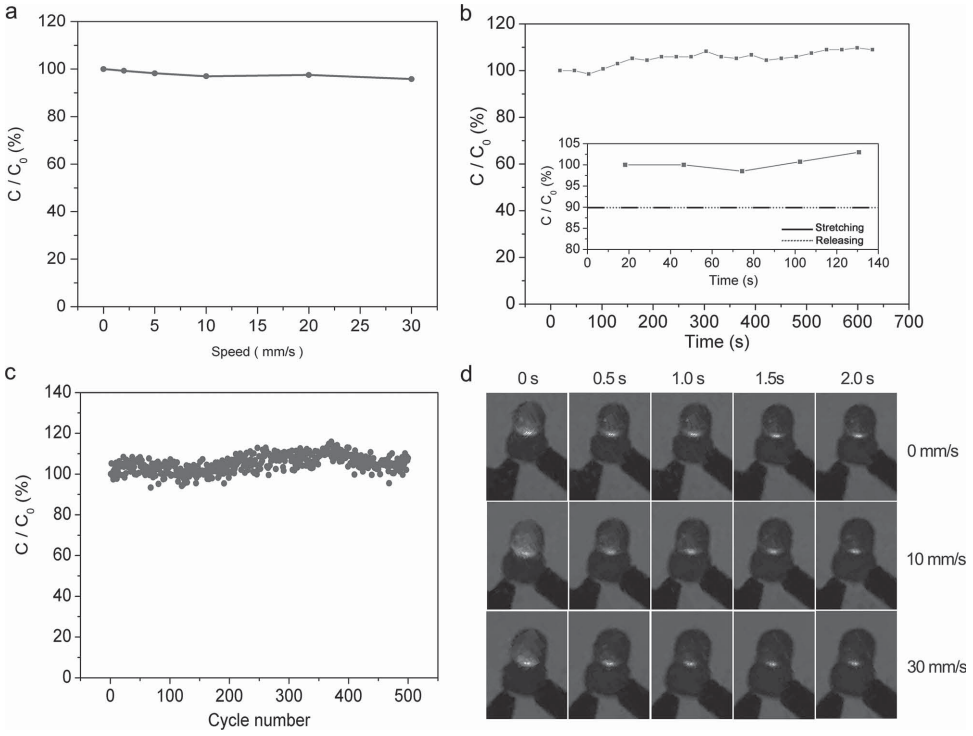

Figure 6. a) Dependence of specific capacitance on stretching speed. C_0 and C correspond to specific capacitances at 0 and the other strain, respectively. b) Dependence of specific capacitance on time during stretching and releasing at a speed of 10 mm s^{-1} (inserted, from ~20 to ~130 s). c) Dependence of specific capacitance on stretching and releasing number at a current density of 1 A g^{-1}. d) Photographs of a light emission diode powered by the flexible and stretchable supercapacitor textile without stretching and with stretching speeds of 10 and 30 mm s^{-1}. For b, c), C_0 and C correspond to specific capacitances before and after stretching, respectively.

the prestretched elastic polymer fiber,[10] and the fabrication details are described in the Supporting Information. The synthesis of spinnable CNT arrays that had been used to produce the aligned CNT sheet was synthesized by chemical vapor deposition.[20–22] The diameter calculation of the superelastic fiber is discussed in the Supporting Information.

Fabrication of SFS: PANI was electrodeposited onto aligned CNT sheets through an electropolymerization of aniline at a potential of 0.75 V in an aqueous solution of aniline (0.1 M) and H_2SO_4 (1 M) using potassium chloride-saturated Ag/AgCl as a reference electrode and platinum wire as the counter electrode. [5] A PVA gel electrolyte was prepared by mixing a PVA aqueous solution and H_3PO_4 with the PVA/H_3PO_4 weight ratio of 1/1.5.[28] An SFS was fabricated by first coating the PVA gel electrolyte onto the aligned CNT/PANI composite on the polymer fiber, wrapping another CNT/PANI sheet after drying of the PVA gel electrolyte and finally coating the PVA gel electrolyte again. For the characterization convenience, the ends of two electrodes were connected to the external circuit by copper wires (Figure S25, Supporting Information). The calculations on the weight of the PANI/CNT composite and specific capacitance of the device are described in the Supporting Information.

Supporting Information

Supporting Information is available from the Wiley Online Library or from the author.

Acknowledgements

Z. Z. and J. D. contributed equally to this work. This work was supported by MOST (2011CB932503), NSFC (21225417), STCSM (12 nm 0503200), the Fok Ying Tong Education Foundation, the Program for Special Appointments of Professors at Shanghai Institutions of Higher Learning, and the Program for Outstanding Young Scholars from the Organization Department of the CPC Central Committee.

Received: October 3, 2014
Published online: November 25, 2014

[1] D. Zou, Z. Lv, X. Cai, S. Hou, *Nano Energy* **2012**, *1*, 273.
[2] X. Xiao, T. Li, P. Yang, Y. Gao, H. Jin, W. Ni, W. Zhan, X. Zhang, Y. Cao, J. Zhong, L. Gong, W. C. Yen, W. Mai, J. Chen, K. Huo, Y. L. Chueh, Z. L. Wang, J. Zhou, *ACS Nano* **2012**, *6*, 9200.
[3] B. Weintraub, Y. Wei, Z. L. Wang, *Angew. Chem. Int. Ed.* **2009**, *48*, 8981.
[4] T. Chen, L. Qiu, Z. Yang, H. Peng, *Chem. Soc. Rev.* **2013**, *42*, 5031.
[5] H. Lin, L. Li, J. Ren, Z. Cai, L. Qiu, Z. Yang, H. Peng, *Sci. Rep.* **2013**, *3*, 1353.
[6] L. Hu, M. Pasta, F. L. Mantia, L. Cui, S. Jeong, H. D. Deshazer, J. W. Choi, S. M. Han, Y. Cui, *Nano Lett.* **2010**, *10*, 708.
[7] C. Choi, J. A. Lee, A. Y. Choi, Y. T. Kim, X. Lepro, M. D. Lima, R. H. Baughman, S. J. Kim, *Adv. Mater.* **2014**, *26*, 2059.
[8] Y. H. Kwon, S. W. Woo, H. R. Jung, H. K. Yu, K. Kim, B. H. Oh, S. Ahn, S. Y. Lee, S. W. Song, J. Cho, H. C. Shin, J. Y. Kim, *Adv. Mater.* **2012**, *24*, 5192.
[9] Z. Zhang, X. Chen, P. Chen, G. Guan, L. Qiu, H. Lin, Z. Yang, W. Bai, Y. Luo, H. Peng, *Adv. Mater.* **2014**, *26*, 466.
[10] Z. Yang, J. Deng, X. Sun, H. Li, H. Peng, *Adv. Mater.* **2014**, *26*, 2643.
[11] H. Lin, W. Weng, J. Ren, L. Qiu, Z. Zhang, P. Chen, X. Chen, J. Deng, Y. Wang, H. Peng, *Adv. Mater.* **2013**, *26*, 1217.
[12] T. Chen, L. Qiu, Z. Yang, Z. Cai, J. Ren, H. Li, H. Lin, X. Sun, H. Peng, *Angew. Chem. Int. Ed.* **2012**, *51*, 11977.

[13] K. S. Kim, Y. Zhao, H. Jang, S. Y. Lee, J. M. Kim, K. S. Kim, J. H. Ahn, P. Kim, J. Y. Choi, B. H. Hong, *Nature* **2009**, *457*, 706.
[14] D. Kim, G. Shin, Y. J. Kang, W. Kim, J. S. Ha, *ACS Nano* **2013**, *7*, 7975.
[15] D. J. Lipomi, B. C. Tee, M. Vosgueritchian, Z. Bao, *Adv. Mater.* **2011**, *23*, 1771.
[16] J. A. Rogers, T. Someya, Y. Huang, *Science* **2010**, *327*, 1603.
[17] Z. Yang, J. Deng, X. Chen, J. Ren, H. Peng, *Angew. Chem. Int. Ed.* **2013**, *52*, 13453.
[18] C. Yu, C. Masarapu, J. Rong, B. Wei, H. Jiang, *Adv. Mater.* **2009**, *21*, 4793.
[19] X. Li, T. Gu, B. Wei, *Nano Lett.* **2012**, *12*, 6366.
[20] M. Zhang, K. R. Atkinson, R. H. Baughman, *Science* **2004**, *306*, 1358.
[21] L. Qiu, X. Sun, Z. Yang, W. Guo, H. Peng, *Acta Chim. Sinica* **2012**, *70*, 1523.
[22] H. Peng, X. Sun, F. Cai, X. Chen, Y. Zhu, G. Liao, D. Chen, Q. Li, Y. Lu, Q. Jia, *Nat. Nanotechnol.* **2009**, *4*, 738.
[23] K. Wang, Q. Meng, Y. Zhang, Z. Wei, M. Miao, *Adv. Mater.* **2013**, *25*, 1494.
[24] C. Choi, J. A. Lee, A. Y. Choi, Y. T. Kim, X. Lepró, M. D. Lima, R. H. Baughman, S. J. Kim, *Adv. Mater.* **2014**, *26*, 2059.
[25] T. Yamada, Y. Hayamizu, Y. Yamamoto, Y. Yomogida, A. Izadi-Najafabadi, D. N. Futaba, K. Hata, *Nat. Nanotechnol.* **2011**, *6*, 296.
[26] X. Zhang, Q. Li, Y. Tu, Y. Li, J. Y. Coulter, L. Zheng, Y. Zhao, Q. Jia, D. E. Peterson, Y. Zhu, *Small* **2007**, *3*, 244.
[27] J. N. Wang, X. G. Luo, T. Wu, Y. Chen, *Nat. Commun.* **2014**, *5*, 3848.
[28] C. Zhao, C. Wang, Z. Yue, K. Shu, G. G. Wallace, *ACS Appl. Mat. Interfaces* **2013**, *5*, 9008.
[29] X. Chen, L. Qiu, J. Ren, G. Guan, H. Lin, Z. Zhang, P. Chen, Y. Wang, H. Peng, *Adv. Mater.* **2013**, *25*, 6436.
[30] T. Chen, Y. Xue, A. K. Roy, L. Dai, *ACS Nano* **2013**, *8*, 1039.
[31] Y. Meng, Y. Zhao, C. Hu, H. Cheng, Y. Hu, Z. Zhang, G. Shi, L. Qu, *Adv. Mater.* **2013**, *25*, 2326.
[32] K. Wang, Q. Meng, Y. Zhang, Z. Wei, M. Miao, *Adv. Mater.* **2013**, *25*, 1494.
[33] J. Ren, L. Li, C. Chen, X. Chen, Z. Cai, L. Qiu, Y. Wang, X. Zhu, H. Peng, *Adv. Mater.* **2013**, *25*, 1155.
[34] Y. Li, K. Sheng, W. Yuan, G. Shi, *Chem. Commun.* **2013**, *49*, 291.
[35] L. Kou, T. Huang, B. Zheng, Y. Han, X. Zhao, K. Gopalsamy, H. Sun, C. Gao, *Nat. Commun.* **2014**, *5*, 3754.
[36] P. Yang, W. Mai, *Nano Energy* **2014**, *8*, 274.
[37] M. D. Stoller, R. S. Ruoff, *Energy Environ. Sci.* **2010**, *3*, 1294.
[38] S. R. Sivakkumar, W. J. Kim, J.-A. Choi, D. R. MacFarlane, M. Forsyth, D.-W. Kim, *J. Power Sources* **2007**, *171*, 1062.
[39] C.-C. Hu, W.-Y. Li, J.-Y. Lin, *J. Power Sources* **2004**, *137*, 152.
[40] Z. Lei, N. Christov, X. S. Zhao, *Energy Environ. Sci.* **2011**, *4*, 1866.
[41] D. P. Dubal, S. H. Lee, J. G. Kim, W. B. Kim, C. D. Lokhande, *J. Mater. Chem.* **2012**, *22*, 3044.
[42] P. Xu, T. Gu, Z. Cao, B. Wei, J. Yu, F. Li, J.-H. Byun, W. Lu, Q. Li, T.-W. Chou, *Adv. Energy Mater.* **2014**, *4*, 1300759.
[43] Y. Xie, Y. Liu, Y. Zhao, Y. H. Tsang, S. P. Lau, H. Huang, Y. Chai, *J. Mater. Chem. A* **2014**, *2*, 9142.
[44] B. Yue, C. Wang, X. Ding, G. G. Wallace, *Electrochim. Acta* **2012**, *68*, 18.
[45] C. Yu, C. Masarapu, J. Rong, B. Wei, H. Jiang, *Adv. Mater.* **2009**, *21*, 4793.
[46] Z. Niu, H. Dong, B. Zhu, J. Li, H. H. Hng, W. Zhou, X. Chen, S. Xie, *Adv. Mater.* **2013**, *25*, 1058.
[47] G. Yu, L. Hu, M. Vosgueritchian, H. Wang, X. Xie, J. R. McDonough, X. Cui, Y. Cui, Z. Bao, *Nano Lett.* **2011**, *11*, 2905.
[48] J. Bae, M. K. Song, Y. J. Park, J. M. Kim, M. Liu, Z. L. Wang, *Angew. Chem. Int. Ed.* **2011**, *50*, 1683.